Discovery and molecular basis of potent noncovalent inhibitors of fatty acid amide hydrolase (FAAH)

Xiaoshan Min[a], Stephen T. Thibault[a], Amy C. Porter[b], Darin J. Gustin[c], Timothy J. Carlson[d], Haoda Xu[a], Michelle Lindstrom[b], Guifen Xu[d], Craig Uyeda[d], Zhihua Ma[c], Yihong Li[c], Frank Kayser[c], Nigel P. C. Walker[a], and Zhulun Wang[a,1]

[a]Departments of Molecular Structure; [b]Neuroscience; [c]Chemistry; and [d]Pharmacokinetics and Drug Metabolism, Amgen Inc., 1120 Veterans Boulevard, South San Francisco, CA 94080

Edited* by Robert M. Stroud, University of California, San Francisco, CA, and approved March 18, 2011 (received for review October 29, 2010)

Fatty acid amide hydrolase (FAAH), an amidase-signature family member, is an integral membrane enzyme that degrades lipid amides including the endogenous cannabinoid anandamide and the sleep-inducing molecule oleamide. Both genetic knock out and pharmacological administration of FAAH inhibitors in rodent models result in analgesic, anxiolytic, and antiinflammatory phenotypes. Targeting FAAH activity, therefore, presents a promising new therapeutic strategy for the treatment of pain and other neurological-related or inflammatory disorders. Nearly all FAAH inhibitors known to date attain their binding potency through a reversible or irreversible covalent modification of the nucleophile Ser241 in the unusual Ser-Ser-Lys catalytic triad. Here, we report the discovery and mechanism of action of a series of ketobenzimidazoles as unique and potent noncovalent FAAH inhibitors. Compound 2, a representative of these ketobenzimidazoles, was designed from a series of ureas that were identified from high-throughput screening. While urea compound 1 is characterized as an irreversible covalent inhibitor, the cocrystal structure of FAAH complexed with compound 2 reveals that these ketobenzimidazoles, though containing a carbonyl moiety, do not covalently modify Ser241. These inhibitors achieve potent inhibition of FAAH activity primarily from shape complementarity to the active site and through numerous hydrophobic interactions. These noncovalent compounds exhibit excellent selectivity and good pharmacokinetic properties. The discovery of this distinctive class of inhibitors opens a new avenue for modulating FAAH activity through nonmechanism-based inhibition.

structure-based design | medicinal chemistry

Fatty acid amides (FAAs) represent a class of lipid signaling molecules that modulate a wide range of physiological processes in the central nervous system (1). As a prominent member of the FAA family, the endogenous cannabinoid anandamide, also known as N-arachidonoylethanolamine or AEA, produces its neurotransmitting effects by binding to and activating two G protein-coupled cannabinoid receptors (i.e., CB1 in the central nervous system and CB2 in the periphery) (2). Previous studies have shown that the effects of anandamide include neurological pain suppression, antiproliferation of cancer cells, enhancement of feeding behavior, and generation of motivation and pleasure (3–7). Endogenous oleamide (*cis*-9,10-octadecenoamide), also known as a sleep-inducing molecule in the FAA family, was found in the cerebrospinal fluid of sleep-deprived animals (8, 9). In addition, other neurological activities have been associated with oleamide, including regulation of memory processes, body temperature, and locomotor activity (10–12). However, the actions of these lipid messengers are ephemeral because of the hydrolytic activity of a number of enzymes including fatty acid amide hydrolase (FAAH). FAAH is an integral membrane enzyme that degrades these lipid amides (13–17) and thus terminates their activities. Inhibition of FAAH activity provides an attractive approach for preventing the deactivation of these endogenous lipid messengers and thereby increasing their half-life in various tissues.

FAAH belongs to the amidase signature (AS) superfamily of serine hydrolases (18) and is the only characterized member in mammals (4). This class of enzyme is defined by a highly conserved primary sequence stretch rich in serine and glycine residues and characterized by a unique Ser-Ser-Lys catalytic triad (18–20). FAAH knockout mice had endogenous levels of anandamide elevated more than 15 fold in the nervous system (21). These mice showed reduced inflammation in a number of models and exhibited reduced pain sensation in various tests (22–24). Similarly, pharmacological administration of FAAH inhibitors also exhibited reduced pain sensation and inflammation in mice (25, 26). Targeting FAAH, therefore, presents a potential new therapeutic strategy for the treatment of pain and inflammation. Additionally, FAAH inhibition may be useful for alleviating sleep disorders and certain neurological-related conditions.

A number of FAAH inhibitors have been identified to date. The initial FAAH inhibitors, such as ATMK (arachidonoyl trifluoromethyl ketone) and MAFP (methoxy arachidonyl fluorophosphonate), are based on the structures of oleamide and AEA (Fig. S1 *A* and *B*), and have a serine reactive electrophile in place of the substrate amide. Because of their reactive functional groups, these inhibitors are all mechanism based and are not specific for a number of serine hydrolases (15, 27). More recently, several new classes of inhibitors (Fig. S1*C*) have been reported, including α-ketoheterocycles (OL-135) (28), carbamates (URB597) (29), piperidine ureas (PF-750 and PF-3845) (30), arylureas (LY2183240) (31, 32), and others (32–34). These recently reported inhibitors are highly potent and selective, with some of them demonstrating in vivo efficacy (26, 35). The inhibitor cocrystal structures were also reported for MAFP with rat FAAH, and PF-750, PF-3845, URB597, and OL-135 with humanized rat FAAH (36–41). However, like ATMK and MAFP, most of the inhibitors disclosed so far rely on covalent modification of the catalytic serine 241 in the active site, either by forming a stable acyl-enzyme adduct or a hemi-acetal with Ser241, which is stabilized by the oxyanion hole. Few examples of potent noncovalent inhibitors have been reported in the literature (33), and it is worth noting that no noncovalent compounds with cellular activity have yet been disclosed.

In an effort to identify unique, potent, and selective inhibitors of FAAH, a high-throughput screening (HTS) campaign was conducted against an in-house small molecule library. A series of

Author contributions: X.M., F.K., N.P.C.W., and Z.W. designed research; X.M., S.T.T., A.C.P., D.J.G., T.J.C., H.X., M.L., G.X., C.U., and Z.W. performed research; Z.M. and Y.L. contributed new reagents/analytic tools; X.M., A.C.P., T.J.C., and Z.W. analyzed data; and X.M., A.C.P., D.J.G., T.J.C., N.P.C.W., and Z.W. wrote the paper.

Conflict of interest statement: All authors are employees of Amgen Inc.

*This Direct Submission article had a prearranged editor.

Freely available online through the PNAS open access option.

Data deposition: The atomic coordinates and structure factors have been deposited in the RCSB Protein Data Bank, www.rcsb.org, (Accession codes 3QJ8, 3QJ9, and 3QKV).

[1]To whom correspondence should be addressed. E-mail: zwang@amgen.com.

This article contains supporting information online at www.pnas.org/lookup/suppl/doi:10.1073/pnas.1016167108/-/DCSupplemental.

BIOCHEMISTRY

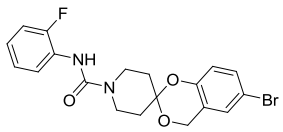

Compound **1**
IC_{50} = 0.036 μM (rat FAAH)
IC_{50} = 0.005 μM (human FAAH)

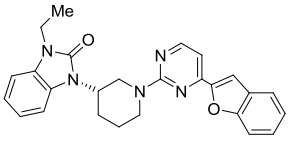

Compound **2**
IC_{50} = 0.10 μM (rat FAAH)
IC_{50} = 0.028 μM (human FAAH)

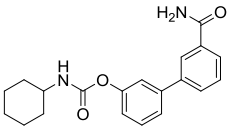

URB597
IC_{50} = 0.003 μM (rat FAAH)
IC_{50} = 0.004 μM (human FAAH)

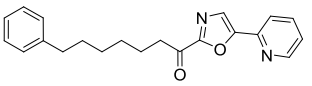

OL-135
IC_{50} = 0.025 μM (rat FAAH)
IC_{50} = 0.016 μM (human FAAH)

Fig. 1. Chemical structures of FAAH inhibitors.

urea-based compounds exemplified by compound **1** (Fig. 1) were identified as potent inhibitors of both rat and human FAAH. Cocrystal structural characterization of compound **1** revealed that it is a substrate type suicide inhibitor. As part of a medicinal chemistry effort to improve potency and selectivity of the HTS hits, we conceived of reducing the reactivity of the urea electrophile to generate inhibitors with a reversible covalent or noncovalent inhibition mechanism. This structure-based design effort led to the successful discovery of a series of ketobenzimidazoles, represented by compound **2** (Fig. 1), as unique FAAH inhibitors. Through extensive structural, mechanistic, and pharmacological characterization, we demonstrated that these ketobenzimidazoles are noncovalent FAAH binders with inhibition potencies comparable to those of covalent inhibitors. In addition, these inhibitors possess excellent selectivity and pharmacokinetic properties. This report describes the discovery and mechanism of action studies of a piperidine-urea identified by HTS as well as a unique series of potent noncovalent FAAH inhibitors.

Results

Active Site Native Conformation Revealed by Apo Rat FAAH Crystal Structure. To elucidate the molecular basis of inhibition for the HTS hits, we carried out X-ray structural analysis of apo FAAH as well as FAAH in complex with various inhibitors. Because of the difficulties in expressing sufficient amounts of soluble human FAAH enzyme, we used an N-terminal truncated form of rat FAAH for the X-ray crystallographic studies. Note that human and rat FAAH have the same catalytic triad of Ser241-Ser217-Lys142 and also have a similar active site that bears six mutations from rat to human (i.e., Leu192Phe, Phe194Tyr, Ala377Thr, Ser435Asn, Ile491Val, and Val495Met).

We first solved the apo structure of rat FAAH to a resolution of 2.9 Å, which served as a basis for the elucidation of inhibitor-protein interactions. The overall structure of the FAAH protein resembles those previously reported (36–41). The core structure of the FAAH monomer adopts an α/β fold with a twisted 11-strand β-sheet in the center and 24 α-helices surrounding the sheet (Fig. 2*A*), resembling that of the first AS structure of bacterial malonamidase E2 (18–20). The active site is located in the center cavity defined by an atypical Ser-Ser-Lys catalytic triad which comprises the catalytic nucleophile residue Ser241 along with residues Ser217 and Lys142. There are three channels and cavities leading away from the catalytic core (Fig. 2*B*), known as (*i*) the membrane access channel (MAC), which directs to a protein surface opening facing the membrane bilayer; (*ii*) the acyl-chain binding pocket (ABP), which is thought to bind the substrate acyl chain during the reaction; and (*iii*) the cytosolic port (CP), which is believed to serve as the passageway for water molecules to access the catalytic center as well as the exit route

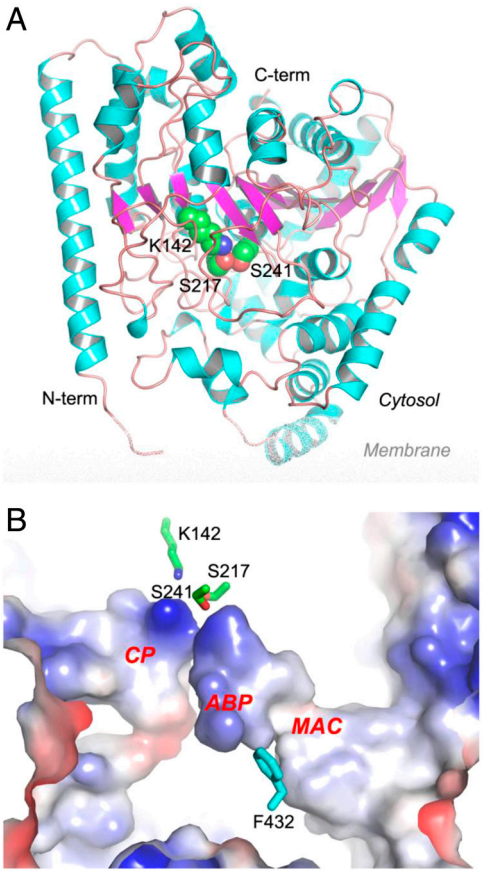

Fig. 2. Crystal structure of apo rat FAAH. (*A*) Overall structure of FAAH monomer in ribbon representation with the center β-sheet colored in magenta, surrounding α-helices in cyan, and loops in pink. The catalytic triad of Ser241-Ser217-Lys142 is shown in spheres with atomic color of carbon in green, oxygen in red, and nitrogen in blue. (*B*) Active site of FAAH in electrostatic surface representation. Three major cavities in the active site are highlighted as the membrane access channel (MAC), the acyl-chain binding pocket (ABP), and the cytosolic port (CP). The catalytic triad and residue Phe432 are shown in sticks.

for the polar reaction products (36). In the proximal portion of the active site, the MAC and the ABP are amalgamated into one unified section. Together, the MAC and ABP form a wide channel that is predominantly hydrophobic in nature on one side and moderately polar on the other side.

The active-site areas of the apo structure are identical to those of reported structures that are complexed with ligand, except for the side chains of a few residues, in particular Phe432. Alternate side chain conformations of Phe432 have also been seen in different FAAH structures that have been complexed with ligand. Some nearby residues show coordinated movements following a Phe432 side chain conformational shift, most notably Met436 and Phe381. Our apo FAAH structure has established the native conformation of Phe432 whose side chain orients toward the acyl-chain binding pocket (Fig. 2*B*), resulting in a rather large and broad MAC and a short and narrow ABP. Such structural features in the active site for apo FAAH provide strong support for the hypothesis of the MAC being the putative entryway for various substrates.

Cocrystal Structure Characterization of Compound 1 as a Suicide Substrate Inhibitor. Compound **1** is a representative of a series of piperazine- and piperidine-containing urea compounds that were identified through the HTS campaign as potent inhibitors of rat and human FAAH (Fig. 1). To understand the molecular recognition of this series of compounds toward FAAH, a cocrystal

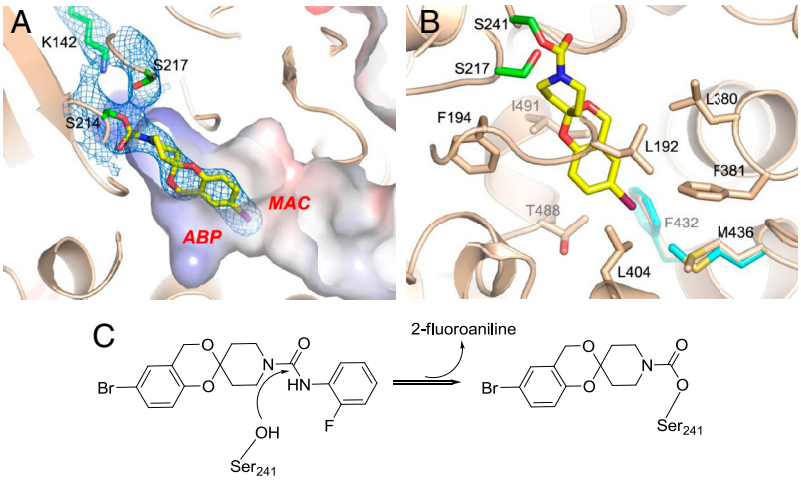

Fig. 3. Binding of compound **1** in the active site of rat FAAH. (*A*) Compound **1** in the active site, with electron density shown as a blue mesh and contoured at a level of 1σ from a 2Fo-Fc map. Compound **1** is shown in sticks with atomic color of carbon in yellow, oxygen in red, nitrogen in blue, and bromine in deep purple. The catalytic triad is shown in sticks with carbon in green. The protein is shown in both ribbon and electrostatic molecular surface representations. (*B*) Compound **1** binding pocket with surrounding residues shown in sticks with carbon atom colored wheat. The corresponding residues, Phe432 and Met436, from the apo FAAH structure are shown in color cyan. (*C*) Mechanism of the covalent modification of FAAH by compound **1**.

structure of compound **1** in complex with rat FAAH was determined to a resolution of 3.1 Å. The well defined electron density for compound **1** revealed ligand binding at the active site in the united section of the MAC and ABP (Fig. 3*A*). It is interesting to note that compound **1** forms a covalent complex with the protein through a carbamate linkage between the catalytic nucleophile Ser241 and the spiro-benzodioxine piperidine portion of the ligand (Fig. 3*A*). The 2-fluoroaniline group is cleaved and is not observed in the structure. The spiro-benzodioxine piperidine moiety is buried in the united section of the MAC and ABP and makes favorable van der Waals contacts with the side chains of a number of hydrophobic residues that line the pocket, including Leu192, Phe194, Leu380, Ile491, Leu404, Thr488, Phe381, Phe432, and Met436 (Fig. 3*B*).

In comparison with the apo structure, the active site shows very few changes. The only notable change is in the side chain conformation of residue Met436 whose Cε atom rotates about 90° to accommodate the bromine atom of compound **1** (Fig. 3*B*). Here, we noticed that Phe432 in the compound **1** cocrystal structure adopts the same conformation as in the apo form. When compared with the reported structures of arachidonyl inhibitor MAFP in rat FAAH (PDB code: 1MT5) and piperidine-urea compound PF-750 in a humanized rat FAAH chimera (PDB code: 2VYA) (36–38), compound **1** shows the same covalent mode of inactivation, in which the urea carbonyl is attacked by Ser241, despite the evident difference in the chemical structures of these covalent adducts. Furthermore, the adducts from these ligands, attached to the catalytic Ser241, follow a similar path toward the united portion of the MAC and ABP and make extensive van der Waals contacts with numerous hydrophobic residues in this proximal portion of the active site.

In summary, the structural data revealed that compound **1** inhibits FAAH through urea carbonyl acylation of the catalytic nucleophile Ser241 with the 2-fluoroaniline moiety as the leaving group (Fig. 3*C*). Compound **1** behaves as a suicide substrate inhibitor.

Structure-Based Discovery and Characterization of Unique Noncovalent FAAH-Inhibitor Compound 2. Following the characterization of the HTS lead compound **1**, we initiated a structure-based medicinal chemistry effort to design unique active-site inhibitors. We were particularly interested in noncovalent or reversible covalent compounds, as they might bring enhanced selectivity and fewer unwanted side effects than any of the known covalent inhibitors. One strategy was to introduce steric bulk α to the carbonyl to reduce its susceptibility to hydrolysis. Various bicyclic and spirocyclic ureas and lactams were designed, synthesized, and then characterized through cocrystal structure analysis. The details of the medicinal chemistry effort are described elsewhere (44). A series of ketobenzimidazoles as represented by compound **2** was identified (Fig. 1). Compound **2** demonstrated potent FAAH inhibition with an IC_{50} of 28 nM toward human FAAH and 100 nM toward rat FAAH.

In part to elucidate the molecular mechanism of FAAH inhibition by compound **2**, we determined the cocrystal structure of compound **2** complexed with rat FAAH at 2.3 Å resolution. The well defined electron density maps showed unambiguously the binding of the compound at the active site (Fig. 4*A*). It was surprising that compound **2**, which contains a carbonyl group, does not form a covalent interaction with the catalytic Ser241 (Fig. 4*A*). In addition, the cocrystal structure revealed an unexpected and unique binding mode for compound **2**. The urea carbonyl of

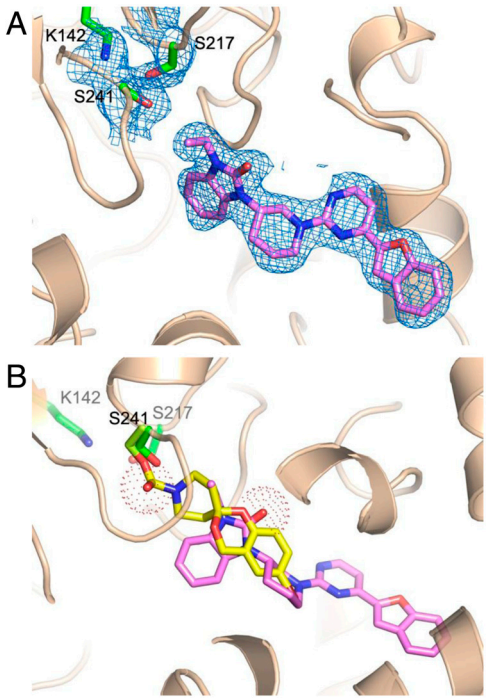

Fig. 4. Binding of compound **2** in the active site of FAAH. (*A*) Electron density contoured at 1σ from a 2Fo-Fc map for compound **2**, Ser241 and Ser217 of the catalytic triad are shown as a blue mesh. Compound **2** is shown in sticks with carbon in magenta, and the catalytic residues are in sticks with carbon in green. The protein is shown in ribbon representation. (*B*) Overall binding of compound **2** in the active site, with compound **1** (with carbon in yellow) overlaid. The protein is shown in ribbons, and the red dotted van der Waals surfaces highlight the different binding sites of the carbonyl oxygen in the two compounds.

compound **2** is positioned and oriented very differently from that of lead compound **1** (Fig. 4*B*). Instead of forming a covalent complex with catalytic residue Ser241, compound **2** locates to the more distal portion of the active site. The distance between the keto carbonyl and the hydroxyl of Ser241 is about 6.3 Å. The compound occupies the united section of the MAC and ABP and then further extends to the long MAC or substrate entry channel (Fig. 4*B*). In addition, a water molecule is observed in the oxyanion hole, further indicating that the enzyme remains in the nonmodified form.

To confirm that the structure is not an artifact of the crystallization condition, we incubated FAAH with compound **2** at enzyme assay conditions for 1 h at 37 °C before setting up crystallization trays. The structure from the preincubated FAAH reveals exactly the same noncovalent binding mode, confirming that compound **2** is unable to form a covalent adduct to the protein. Furthermore, we also incubated the racemate of compound **2** with FAAH under the same condition and solved the cocrystal structure. The electron density clearly demonstrated that only the S-enantiomer was present in the structure.

The high resolution cocrystal structure of compound **2** complexed with rat FAAH allowed us to analyze the key molecular interactions between the inhibitor and the protein in atomic detail. Overall, the interactions between compound **2** and FAAH are predominantly hydrophobic in nature. The ketobenzimidazole moiety of compound **2** is sandwiched between two loops: a loop between residues Ile238 and Ser241, which forms part of the oxyanion hole, and a loop between residues Leu192 and Phe194 (Fig. 5*A*). The ethyl moiety fits snuggly in a small cavity formed by Gly239, Gly240, Ser241, and a water molecule in the oxyanion hole at one side, and Phe244 and Phe194 at the other side (Fig. 5 *A* and *B*). The carbonyl group makes no direct polar interactions with the protein. Instead, the oxygen accepts a hydrogen bond from a water molecule and makes van der Waals contacts with the edge of the Phe194 aromatic ring (Fig. 5*A*). Indeed, replacement of the carbonyl group with a methyl group generated a compound that adopts a similar binding mode to compound **2** and maintains similar potency against FAAH (44), suggesting that the water-mediated hydrogen bond interaction observed for the carbonyl is not critical for the inhibitor binding. The phenyl portion of the benzimidazole fits in a small hydrophobic pocket that is defined by four residues (i.e., Leu192, Ile238, Leu380, and Phe381) (Fig. 5*A*). To accommodate the phenyl ring, Leu192 adopts an alternate side chain conformation than that seen in apo and other complex structures (Fig. 5 *A* and *B*). Apparently, none of the other reported inhibitors access this pocket that in fact results from the swing of the Leu192 side chain upon compound **2** binding.

The piperidine ring has an almost perpendicular orientation relative to the benzimidazole ring (Fig. 5*B*). A T-shape conformation is formed, placing the alpha proton and the carbonyl in an eclipsed relationship as one would expect on the basis of the minimization of the 1,3 allylic strain (42). Thus, it appears that the compound binds to FAAH in its preferred solution conformation. Apparently, this T-shape conformation is complementary to the surface of the cavity, providing a near "hand-in-glove" fit. Many favorable van der Waals interactions are observed for the piperidine ring with the residues lining the cavity, including Phe381, Leu404, I491, Phe432, Thr488, and Met436 (Fig. 5*B*). In this region, a conformational shift is also observed for Met436, which has a side chain that is shifted, relative to that in the apo structure, to accommodate the piperidine ring. The rest of the molecule orients almost coplanar with the piperidine ring and occupies the distal portion of the MAC. The pyrimidine and benzofuran portions engage with the protein via a few distinctive interactions (Fig. 5*C*). Among these interactions, a pyrimidyl nitrogen forms a water-mediated hydrogen bond interaction to the carbonyl of Leu192. The tail benzofuran group is sandwiched between Trp531 and Ile407, forming an aromatic C-H-π interaction with the ring of Trp531.

In summary, the structure clearly reveals that compound **2** is a noncovalent FAAH inhibitor that makes no modification to the nucleophile Ser241 and achieves its high potency mainly through shape complementarity to the large substrate-binding pocket in the active site, including the MAC as well as its united section with the ABP (Fig. 5*D*). Compound **2** demonstrates a unique nonmechanism-based inhibition of FAAH activity, which is distinct from almost all known FAAH inhibitors.

Biological Characterization of Noncovalent Compound 2. With structural elucidation of compound **2** as a noncovalent FAAH binder, a series of experiments were performed to examine the inhibition activity of compound **2** in more detail. Following the biochemical inhibition measurement, we carried out whole-cell assays to con-

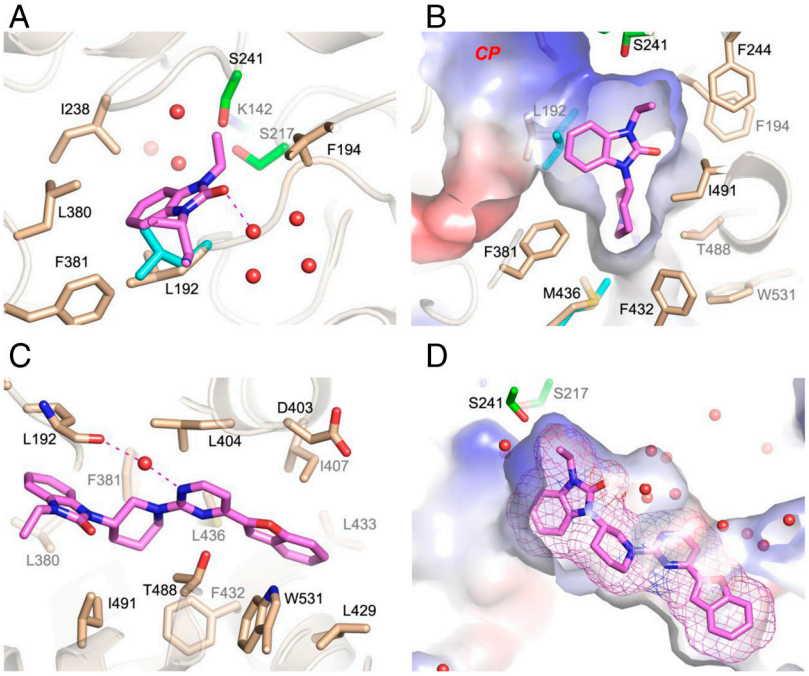

Fig. 5. Inhibitor-protein interactions for compound **2**. (*A*) The binding of the ketobenzimidazole headpiece in the active site of FAAH with compound **2** shown in sticks with carbon in magenta and surrounding residue side chains in wheat sticks. The catalytic triad residues are shown in sticks with carbon in green. The corresponding residue Leu192 in the apo structure is shown in cyan. The water molecules are shown as red spheres. (*B*) The binding of the piperidine ring portion in the active site. The protein is shown in molecular surface representation, and its side chains are in sticks. The corresponding residues Leu192 and M436 in the apo structure are shown in cyan. (*C*) The binding of the pyrimidine and benzofuran tail portion. (*D*) Shape complementarity of compound **2** to the active site. The ligand is shown in both stick and mesh representations, and the protein is shown in molecular surface representation.

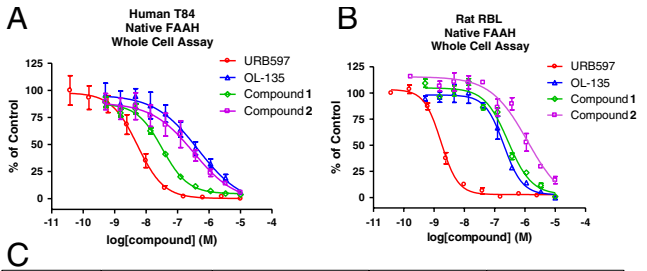

C

Inhibitor	Whole Cell T84 EC_{50} (nM)	Purified Human FAAH EC_{50} (nM)	Whole Cell RBL EC_{50} (nM)	Purified Rat FAAH EC_{50} (nM)
URB597	5.4	4.2	1.7	3.4
OL-135	450	16	200	25
Compound **1**	33	5	276	36
Compound **2**	320	28	951	102

Fig. 6. Pharmacology of compound **1**, compound **2**, URB 597, and OL-135 in human T84 cells (*A* and *C*) and in rat RBL-2H3 cells (*B* and *C*).

firm the cellular-based activities of these noncovalent inhibitors. Fig. 6 shows the inhibition of FAAH activities in both the human tissue T84 cells and rat RBL-2H3 cells by compound **1** and compound **2** as well as OL-135 and URB597. These four compounds represent three distinctive classes of FAAH inhibitors: irreversible covalent (compound **1** and URB597), reversible covalent (OL-135), and reversible noncovalent (compound **2**). Although compound **2** is not covalently attached to FAAH, it still achieves potent cellular FAAH inhibition, with IC_{50}s of 320 nM and 951 nM in human and rat FAAH whole-cell assays, respectively.

Next, we measured activities of these ketobenzimidazoles in a panel of cannabinoid related targets, including CB1, CB2, and VR1. Compound **2** demonstrated an excellent selectivity profile against these targets as well as a selectivity over carboxylesterases which other FAAH inhibitors have been shown to target (Table 1) (43). We further evaluated the pharmacokinetics (PK) of compound **2** in rat, and the results are also shown in Table 1. Compound **2** showed excellent PK properties with a low clearance of 0.4 L/h/Kg and a high bioavailability of 92%, making compound **2** suitable for further in vivo studies.

Discussion

Here we have applied a structure-based approach to facilitate the discovery and mechanism of action studies of a series of ketobenzimidazoles as unique, potent, and selective FAAH inhibitors. The molecular recognition and inhibition mechanism revealed by the three-dimensional ligand-protein complex structure clearly demonstrated that compound **2** represents a class of inhibitors that inactivate FAAH activity without a covalent interaction, while the HTS lead compound **1** is an irreversible covalent modifier.

Table 1. Rat pharmacokinetic parameters and selectivity data of compound 2

Profile	Compound 2
Pharmacokinetics *	
Cl (L/h/Kg) †	0.40
Vdss (L/Kg) †	1.5
Cmax (μM) ‡	4.4
MRT (h) ‡	5.5
F (%)	92
Selectivity	
CB1/2 IC_{50} (μM)	>20/ > 20
VR1 IC_{50} (μM)	>20
% inhibition of rat liver carboxylesterase	<10

*Values are means of three individual test subjects.
†Following 0.5 MPK dosed intravenously.
‡Following 2.0 MPK dosed orally.

We first solved the rat FAAH structure in its apo form, which offered an unbiased insight into the active-site architecture. To date, each of the disclosed FAAH structures is in its ligand-bound form; from the first rat FAAH structure in complex with a substrate-inspired irreversible arachidonyl inhibitor to the more-recent structures including human-rat chimeric FAAH in complex with various inhibitors (36–41). While the main chain of the protein showed very little movement from one inhibitor complex to another, the side chains of a few residues lining the active site were found to be rather flexible. Alternate side chain conformations assumed by these residues, in particular Phe432, which was considered as a dynamic paddle (37), led to the reorganization of the substrate/inhibitor binding cavities, including the MAC and ABP. An "open-channel conformation" was illustrated for OL-135, and a "closed" one was observed for both PF-3845 and MAFP. In the absence of an apo structure, it was not possible to predict whether the open or closed conformation is induced by ligand binding. Here, the apo structure clearly reveals that the open conformation is the genuine native conformation for the enzyme. In this native conformation, the Phe432 side chain projects into the ABP, resulting in a substantially abbreviated ABP and widely expanded MAC (Fig. S2*A*). This observation is consistent with the fact that FAAH recognizes various endogenous lipid substrates with different acyl chains that enter the enzyme through this large and wide MAC. The closed conformation is likely the outcome of the rearrangement of flexible residue side chains upon ligand binding (Fig. S2*B*).

The cocrystal structure of compound **2** in complex with FAAH reveals both the inhibitor binding and inactivation mechanism of FAAH activity. Like all other known inhibitors, compound **2** binds in the large active site. However, the compound adopts a significantly different binding mode than that of other inhibitors, including irreversible covalent binders such as our lead compound **1**, URB597, MAFP and PF-3845, and reversible covalent ones such as OL-135 and its analogs. Notably, compound **2** does not engage in any specific polar interactions with the catalytic core, especially not with the Ser241 nucleophile. When superimposed onto the PF-3845 and OL-135 cocrystal structures (Fig. S3*A*), the headpiece of compound **2**, including the ketobenzimidazole and piperidine rings, occupies the proximal portion of the cavity where the MAC and ABP merge. This pocket has been shown to be populated by the terminal groups of those short inhibitors such as OL-135 and the middle section of longer ones like PF-3845. The tail portion of compound **2**, including the pyrimidine and benzofuran rings, however, takes a completely distinct path from the acyl tail of MAFP and the trifluoromethyl pyridyl group of PF-3845. Both MAFP and PF-3845 pack their tail portions in the ligand induced, enlarged ABP as a result of the side chain swing of Phe432 plus the coordinated movements of a few nearby residues, including Met436. The tailpiece of compound **2** resides in the distal MAC which has not been exploited previously by other inhibitors, virtually blocking the substrate entryway completely.

Various FAAH-inhibitor cocrystal structures reveal that the FAAH active site has remarkable flexibility. Alternate side chain conformations assumed by several residues lining the cavity modulate the shape and size of the cavity as well as the partition between the MAC and ABP. The protein retains the open conformation when bound to compound **2**, with Phe432 assuming the same conformation as in the native state. Yet, two residues in the active site adopt alternate side chain conformations relative to the apo structure (i.e., Met436 and Leu192). Whereas the conformational movement illustrated by Met436 is modest, Leu192 shows noteworthy conformational rearrangement that has not been shown with other inhibitors. The side chain of Leu192 swings into the CP side to accommodate the bulky benzimidazole and makes a stacking interaction with the phenyl portion (Fig. S3*B*). It is interesting to note that Leu192 is one of the

six residues that differ between human and rat FAAH. As four of the six mutations (Phe194Tyr, Ala377Thr, Ser435Asn, and Val495Met) are not in close contact with compound **2**, and the Ile491Val change has minimal impact, the Leu192Phe mutation might be largely responsible for the different binding affinities of compound **2** in rat and human FAAH. When we modeled Leu192Phe to mimic the human enzyme, Phe192 made a good aromatic π-π stacking interaction with the phenyl portion in the benzimidazole ring (Fig. S3*B*), which might contribute to the overall binding energy and thus the higher potency of compound **2** for human FAAH.

The therapeutic potential of FAAH inhibition has drawn considerable interest for the design of potent and selective FAAH inhibitors. Several chemical classes have been discovered to date (34); however, nearly all of them are mechanism based, bear reactive carbonyls, and act as either reversible or irreversible covalent modifiers of the catalytic serine. Here we disclose a series of potent and selective ketobenzimidazoles as a unique class of noncovalent FAAH inhibitors. These inhibitors achieve inhibition of FAAH activity by extensive hydrophobic interactions resulting from shape complementarity to the large active site from the proximal portion to the distal MAC. Further in vivo evaluation of compound **2** and its analogues is underway.

Methods

Rat and human FAAH proteins were expressed in *Escherichia coli* and purified by Ni affinity column and glutathione sepharose column respectively. Both native crystals and compound cocrystals were grown using the hanging drop vapor diffusion method. X-ray diffraction datasets were collected on both a home X-ray source and a synchrotron source at the Advanced Light Source (ALS) (Berkeley, CA). The structure was solved by the molecular replacement method (Table S1). FAAH inhibition was determined by measuring production of fluorescent aminomethyl coumarin by UV absorbance at 460 nm. Pharmacokinetic samples were measured by reverse-phase liquid chromatography with tandem mass spectrometry (MS). Detailed methods are described in *SI Text*.

ACKNOWLEDGMENTS. We thank Bob Fremeau and Narender Gavva for assisting the selectivity experiments, and Scott Silbiger for editing the manuscript. The ALS is supported by the Department of Energy under Contract No. DE-AC03-76SF00098 at the Lawrence Berkeley National Laboratory.

1. Di Marzo V (1998) "Endocannabinoids" and other fatty acid derivatives with cannabimimetic properties: biochemistry and possible physiopathological relevance. *Biochim Biophys Acta* 1392:153–175.
2. Devane WA, et al. (1992) Isolation and structure of a brain constituent that binds to the cannabinoid receptor. *Science* 258:1946–1949.
3. De Petrocellis L, et al. (1998) The endogenous cannabinoid anandamide inhibits human breast cancer cell proliferation. *Proc Natl Acad Sci USA* 95:8375–8380.
4. McKinney MK, Cravatt BF (2005) Structure and function of fatty acid amide hydrolase. *Annu Rev Biochem* 74:411–432.
5. Smith PB, et al. (1994) The pharmacological activity of anandamide, a putative endogenous cannabinoid, in mice. *J Pharmacol Exp Ther* 270:219–227.
6. Walker JM, Huang SM, Strangman NM, Tsou K, Sanudo-Pena MC (1999) Pain modulation by release of the endogenous cannabinoid anandamide. *Proc Natl Acad Sci USA* 96:12198–12203.
7. Williams CM, Kirkham TC (2002) Observational analysis of feeding induced by Delta9-THC and anandamide. *Physiol Behav* 76:241–250.
8. Cravatt BF, et al. (1995) Chemical characterization of a family of brain lipids that induce sleep. *Science* 268:1506–1509.
9. Basile AS, Hanus L, Mendelson WB (1999) Characterization of the hypnotic properties of oleamide. *Neuroreport* 10:947–951.
10. Fedorova I, et al. (2001) Behavioral evidence for the interaction of oleamide with multiple neurotransmitter systems. *J Pharmacol Exp Ther* 299:332–342.
11. Huitron-Resendiz S, Gombart L, Cravatt BF, Henriksen SJ (2001) Effect of oleamide on sleep and its relationship to blood pressure, body temperature, and locomotor activity in rats. *Exp Neurol* 172:235–243.
12. Murillo-Rodriguez E, et al. (2001) Oleamide modulates memory in rats. *Neurosci Lett* 313:61–64.
13. Cravatt BF, et al. (1996) Molecular characterization of an enzyme that degrades neuromodulatory fatty-acid amides. *Nature* 384:83–87.
14. Desarnaud F, Cadas H, Piomelli D (1995) Anandamide amidohydrolase activity in rat brain microsomes. Identification and partial characterization. *J Biol Chem* 270:6030–6035.
15. Deutsch DG, Chin SA (1993) Enzymatic synthesis and degradation of anandamide, a cannabinoid receptor agonist. *Biochem Pharmacol* 46:791–796.
16. Maurelli S, et al. (1995) Two novel classes of neuroactive fatty acid amides are substrates for mouse neuroblastoma "anandamide amidohydrolase". *FEBS Lett* 377:82–86.
17. Ueda N, Kurahashi Y, Yamamoto S, Tokunaga T (1995) Partial purification and characterization of the porcine brain enzyme hydrolyzing and synthesizing anandamide. *J Biol Chem* 270:23823–23827.
18. Chebrou H, Bigey F, Arnaud A, Galzy P (1996) Study of the amidase signature group. *Biochim Biophys Acta* 1298:285–293.
19. Mayaux JF, Cerebelaud E, Soubrier F, Faucher D, Petre D (1990) Purification, cloning, and primary structure of an enantiomer-selective amidase from Brevibacterium sp. strain R312: structural evidence for genetic coupling with nitrile hydratase. *J Bacteriol* 172:6764–6773.
20. Shin S, et al. (2002) Structure of malonamidase E2 reveals a novel Ser-cisSer-Lys catalytic triad in a new serine hydrolase fold that is prevalent in nature. *EMBO J* 21:2509–2516.
21. Cravatt BF, et al. (2001) Supersensitivity to anandamide and enhanced endogenous cannabinoid signaling in mice lacking fatty acid amide hydrolase. *Proc Natl Acad Sci USA* 98:9371–9376.
22. Cravatt BF, et al. (2004) Functional disassociation of the central and peripheral fatty acid amide signaling systems. *Proc Natl Acad Sci USA* 101:10821–10826.
23. Lichtman AH, Shelton CC, Advani T, Cravatt BF (2004) Mice lacking fatty acid amide hydrolase exhibit a cannabinoid receptor-mediated phenotypic hypoalgesia. *Pain* 109:319–327.
24. Massa F, et al. (2004) The endogenous cannabinoid system protects against colonic inflammation. *J Clin Invest* 113:1202–1209.
25. Moreira FA, Kaiser N, Monory K, Lutz B (2008) Reduced anxiety-like behavior induced by genetic and pharmacological inhibition of the endocannabinoid-degrading enzyme fatty acid amide hydrolase (FAAH) is mediated by CB1 receptors. *Neuropharmacology* 54:141–150.
26. Lichtman AH, et al. (2004) Reversible inhibitors of fatty acid amide hydrolase that promote analgesia: evidence for an unprecedented combination of potency and selectivity. *J Pharmacol Exp Ther* 311:441–448.
27. Deutsch DG, et al. (1997) Methyl arachidonyl fluorophosphonate: a potent irreversible inhibitor of anandamide amidase. *Biochem Pharmacol* 53:255–260.
28. Boger DL, et al. (2000) Exceptionally potent inhibitors of fatty acid amide hydrolase: the enzyme responsible for degradation of endogenous oleamide and anandamide. *Proc Natl Acad Sci USA* 97:5044–5049.
29. Tarzia G, et al. (2003) Design, synthesis, and structure-activity relationships of alkylcarbamic acid aryl esters, a new class of fatty acid amide hydrolase inhibitors. *J Med Chem* 46:2352–2360.
30. Ahn K, et al. (2007) Novel mechanistic class of fatty acid amide hydrolase inhibitors with remarkable selectivity. *Biochemistry (Mosc)* 46:13019–13030.
31. Alexander JP, Cravatt BF (2006) The putative endocannabinoid transport blocker LY2183240 is a potent inhibitor of FAAH and several other brain serine hydrolases. *J Am Chem Soc* 128:9699–9704.
32. Wang JL, et al. (2009) Structure based design of novel irreversible FAAH inhibitors. *Bioorg Med Chem Lett* 19:5970–5974.
33. Wang X, et al. (2009) Synthesis and evaluation of benzothiazole-based analogues as novel, potent, and selective fatty acid amide hydrolase inhibitors. *J Med Chem* 52:170–180.
34. Seierstad M, Breitenbucher JG (2008) Discovery and development of fatty acid amide hydrolase (FAAH) inhibitors. *J Med Chem* 51:7327–7343.
35. Clapper JR, et al. (2010) Anandamide suppresses pain initiation through a peripheral endocannabinoid mechanism. *Nat Neurosci* 13:1265–1270.
36. Bracey MH, Hanson MA, Masuda KR, Stevens RC, Cravatt BF (2002) Structural adaptations in a membrane enzyme that terminates endocannabinoid signaling. *Science* 298:1793–1796.
37. Mileni M, et al. (2008) Structure-guided inhibitor design for human FAAH by interspecies active site conversion. *Proc Natl Acad Sci USA* 105:12820–12824.
38. Ahn K, et al. (2009) Discovery and characterization of a highly selective FAAH inhibitor that reduces inflammatory pain. *Chem Biol* 16:411–420.
39. Mileni M, et al. (2009) Binding and inactivation mechanism of a humanized fatty acid amide hydrolase by alpha-ketoheterocycle inhibitors revealed from cocrystal structures. *J Am Chem Soc* 131:10497–10506.
40. Mileni M, et al. (2010) Crystal structure of fatty acid amide hydrolase bound to the carbamate inhibitor URB597: discovery of a deacylating water molecule and insight into enzyme inactivation. *J Mol Biol* 400:743–754.
41. Mileni M, et al. (2010) X-ray crystallographic analysis of alpha-ketoheterocycle inhibitors bound to a humanized variant of fatty acid amide hydrolase. *J Med Chem* 53:230–240.
42. Hoffmann RW (1989) Allylic 1,3-strain as a controlling factor in stereoselective transformations. *Chem Rev* 89:1841–1860.
43. Zhang D, et al. (2007) Fatty acid amide hydrolase inhibitors display broad selectivity and inhibit multiple carboxylesterases as off-targets. *Neuropharmacology* 52:1095–1105.
44. Gustin DJ, et al. (2011) Identification of potent, noncovalent fatty acid amide hydrolase (FAAH) inhibitors. *Bioorg Med Chem Lett* 21:2492–2496.